INTERNATIONAL JOURNAL FOR NUMERICAL METHODS IN FLUIDS
Int. J. Numer. Meth. Fluids 2006; **50**:1445–1460
Published online 17 November 2005 in Wiley InterScience (www.interscience.wiley.com). DOI: 10.1002/fld.1114

Numerical investigation of the flow front behaviour in the co-injection moulding process

F. Ilinca*,†, J.-F. Hétu‡ and A. Derdouri§

Industrial Materials Institute, National Research Council, 75 de Mortagne, Boucherville, Que., Canada J4B 6Y4

SUMMARY

This paper presents a three-dimensional (3D) solution algorithm for solving the sequential co-injection moulding process. The flow of skin and core materials inside a rectangular cavity is investigated both numerically and experimentally. A 3D finite element flow analysis code is used to solve the governing equations of the non-isothermal sequential co-injection moulding. The predicted flow front behaviour is compared to the experimental observations for various skin/core volume ratio, injection speed, injection temperature, and core injection delay. Simulation results are in good agreement with experimental data and indicate correctly the trends in solution change when processing parameters are changing. Solutions are also shown for the filling of a spiral-flow mould. The numerical approach is shown to predict the core expansion phase during which the flow front of core and skin materials advance together without breakthrough. Breakthrough phenomena is also predicted and the numerical solution is in good agreement with the experiment. Copyright © 2005 Crown in the right of Canada. Published by John Wiley & Sons, Ltd.

KEY WORDS: co-injection; 3D simulation; finite elements; experimental validation

1. INTRODUCTION

The co-injection process has been known for about twenty years, since Garner and Oxley [1] first patented the process. Also known as sandwich moulding, it consists basically in injecting in the mould cavity more than one plastic material to form a part with skin layers surrounding a core layer. The skin and core materials generally have different properties, but they must have a good adhesion at the interface, be processable in a comparable range of melt temperatures and present similar shrinkage characteristics. The first applications of the new process were

*Correspondence to: F. Ilinca, Industrial Materials Institute, National Research Council, 75 de Mortagne, Boucherville, Que., Canada J4B 6Y4.
†E-mail: florin.ilinca@cnrc-nrc.gc.ca
‡E-mail: jean-francois.hetu@cnrc-nrc.gc.ca
§E-mail: salim.derdouri@cnrc-nrc.gc.ca

Received 20 September 2004
Revised 25 August 2005
Accepted 30 August 2005

to produce less expensive and lighter thick parts by using a foamed or recycled plastic for the core and a virgin plastic for the skin. Various other applications are in use today: skin or core made out of engineering resins to improve physical properties of the part such as strength, heat deflection or weather resistance, improvement of barrier properties of food containers, specifically multi-layer preforms for plastic bottles, and in-mould painting. The techniques of injecting the skin and core materials can be divided into two main methods: the one-channel technique which has a control valve that lets the melts enter the cavity in a sequential order [2], and the simultaneous injection which uses a two-channel nozzle [3]. The shortcomings of the one-channel technique (pressure drop and stagnation at the switchover point resulting in a 'hesitation line' having the shape of a dull ring) have been overcome by the two-channel technique, but the simultaneous injection is more difficult to control and require time-consuming trial and error iterations.

Control of the flow fronts can be achieved by varying the skin/core ratio, processing conditions and rheological properties of the skin and core materials. Previous experimental studies on this subject dealt mostly with the role of the viscosity ratio of the two materials [4, 5]. Few numerical simulations of the co-injection filling process have been attempted in the past decade [6–10]. All of them use the Hele–Shaw approximation (2.5D) to predict the interface evolution between skin and core material during filling for the sequential injection, with the exception of Lee *et al.* [9] who also considered the simultaneous injection. All these studies highlighted the importance of the viscosity ratio and the rate of injection. While for parts with non-uniform thick sections the Hele–Shaw approximation is clearly inappropriate, it is even more inaccurate in predicting the relative material distribution between the skin and core section. As the core polymer penetration is a 3D phenomenon, it is important to provide not only the depth of the core penetration, but also details on the core shape and polymer skin thickness. The limitations of the 2.5D approach for the simulation of the co-injection process and the advantages of the 3D simulation for the solution of such problems are discussed in more detail in Reference [11].

The objective of this work is to present applications of a 3D solution algorithm for the solution of the sequential co-injection moulding process. The numerical predictions are validated experimentally for various moulding conditions. The values of the skin/core ratio, injection speed, melt and mould temperatures are varied in order to gain further basic understanding of the flow behaviour of two polymers during the filling of a mould. The present numerical approach is based on the finite element method. The solution of the 3D equations modelling the momentum, mass and energy conservation is coupled with two front-tracking equations, which are solved for the polymer/air and skin/core polymer interfaces. The polymer melt is considered incompressible and behaving as a generalized Newtonian fluid. Equations are solved using stabilized finite element formulations. Momentum-continuity equations are solved by the Galerkin least-squares (GLS) method [12, 13]. The energy equation is solved using a GLS/GGLS (Galerkin least-squares/Galerkin gradient least-squares) method [12, 14, 15]. The front tracking equations are solved by a streamline upwind Petrov–Galerkin (SUPG) method [12]. The 3D solution algorithm was previously used by the authors to solve the filling and post-filling phases of the injection moulding process [16], the injection of metal powders [17], and the gas-assisted injection moulding [18]. By solving for the true 3D mould filling problem the solution approach will be able to provide accurate and detailed information regarding the shape and size of the core polymer, as well as the thickness of the skin. Those results will be especially useful in critical regions such as near corners, obstacles,

or in regions presenting changes in part thickness. A robust and accurate solution algorithm also provides the framework for detailed analysis of the role played by different parameters determining the final characteristics of the part. In such a way the optimal design of the process is a realizable task.

2. NUMERICAL MODELLING

2.1. Assumptions

The constitutive equations are given to represent the thermal and mechanical behaviour of isotropic amorphous polymers during the filling stage of the injection moulding process. Here are the main considerations behind the choice of model equations described in this section.

The maximum pressure drop encountered during the filling of most plastic parts is about 10^6–10^7 Pa. Considering that the compressibility coefficient of most polymer melts is of the order of $10^{-9}\,\mathrm{Pa}^{-1}$, one can conclude that compressibility effects can be neglected. The polymer melt is thus considered incompressible.

Second, the mechanical behaviour of an amorphous polymer in shear dominated flows (such as in injection moulding and co-injection) can be described reasonably well by a generalized Newtonian fluid model. This assumption has been validated numerically by Baaijens and Douven [19, 20] who showed that flow kinematics predicted by viscoelastic approach do not significantly differ from the one obtained using a generalized Newtonian approach. This is also in agreement with experimental observations of Wimberger-Friedl [21] and Janeschitz-Kriegl [22].

Polymer melts have a surface tension σ between 20 and 50 mN/m [23] and viscosities are of the order of 10^3 Pa s. Velocities at the interface are of the order of 0.02 m/s leading to a Capillary number $Ca = \eta V/\sigma$ of the order of $O(10^3)$. Similar dimensional analysis leads to Reynolds numbers in the range of 10^{-4}–10^{-2}. One can conclude that viscous forces dominate and that both inertia and surface tensions can be neglected in the momentum equation. Meanwhile, given the small thermal conductivity of polymers, the Peclet number takes very large values, in the range of 10^3–10^5, and the inertia has to be taken into account in the energy equation.

2.2. Governing equations

The equations governing the incompressible melt flow are the Stokes and continuity equations

$$0 = -\nabla p + \nabla \cdot [2\eta\dot{\gamma}(\mathbf{u})] \tag{1}$$

$$-\nabla \cdot \mathbf{u} = 0 \tag{2}$$

where $\dot{\gamma}(\mathbf{u}) = (\nabla\mathbf{u} + \nabla\mathbf{u}^{\mathrm{T}})/2$ is the strain rate tensor. Heat transfer is modelled by the energy equation

$$\rho c_p \left(\frac{\partial T}{\partial t} + \mathbf{u} \cdot \nabla T \right) = \nabla \cdot (k \nabla T) + 2\eta\dot{\gamma}^2 \tag{3}$$

In the above equations, t, $\mathbf{u}$, p, T, ρ, η, c_p and k denote time, velocity vector, pressure, temperature, density, viscosity, specific heat and thermal conductivity, respectively.

Table I. Definition of filled (skin/core) and empty regions.

	$F_1 \geqslant F_c$	$F_1 < F_c$
$F_2 \geqslant F_c$	Core polymer	Core breakthrough skin material
$F_2 < F_c$	Skin polymer	Empty (air)

2.3. Front tracking method

The position of the polymer/air and skin/core polymer interfaces is tracked using a pseudo-concentration method [16]. The approach defines smooth functions F_i such that the critical value F_c represents the position of the interface. We consider $i=1$ for the polymer/air interface and $i=2$ for the skin/core interface. A front tracking value greater than F_c denotes a region filled by the respective polymer, while a smaller than F_c value corresponds to an unfilled region. Because two interfaces are present, the various combinations are summarized in Table I. The front tracking technique identifies the skin, core and empty regions. Core breakthrough is also predicted.

At each time step the pseudo-concentration functions tracking the polymer/air and skin/core interfaces are obtained by solving pure advection equations using the velocity field provided by the solution of the momentum-continuity equations

$$\frac{\partial F_i}{\partial t} + \mathbf{u} \cdot \nabla F_i = 0 \tag{4}$$

2.4. Boundary conditions

Appropriate boundary conditions complete the statement of the problem. On the entry section both velocity and temperature are imposed. Filling is performed at constant flow rate as given by the velocity of the screw. The injection is performed using different barrel/screw plasticizing units, therefore the injection speed and temperature may be different for the skin and core materials. A free boundary condition is imposed on the unfilled part of the cavity walls allowing for the formation of the typical fountain flow, whereas no-slip boundary conditions are imposed on the filled part of the boundary. When the cavity is completely filled, the simulation stops as the no-slip boundary condition cannot allow more material to enter the cavity. The heat transfer between the cavity and the mould is given by

$$q = h_c(T - T_{\text{mould}}) \quad \text{on } \Gamma_{\text{mould}} \tag{5}$$

where h_c is a surface heat transfer coefficient and T_{mould} is the mould temperature. For the front tracking function, homogeneous Neumann boundary conditions are considered on all boundaries, except for the entry where Dirichlet conditions are imposed. Entry values change in time and indicate whether skin or core polymers are injected.

2.5. Finite element solution procedure

Model equations are discretized in time using a first-order implicit Euler scheme. Linear continuous shape functions are used for all variables. At each time step, the global system of

equations is solved in a partly segregated manner. The solution algorithm solves separately the systems of equations as follows:

For time smaller than the injection time:

1. Solve the incompressible momentum-continuity equations ($\mathbf{u} - p$).
2. Solve the energy equation (T).
3. Solve the front tracking equation F_1 (polymer/air interface) if skin material is injected, or equations (F_1, F_2) if core material is injected. Check convergence. If converged goto the next time step, otherwise repeat steps 1 to 3.

Steps 1–3 are solved using the last known values of the dependent variables and iterations are made to obtain converged solutions of the coupled system of equations. The finite element formulations of the equations are discussed hereafter.

2.6. *Momentum-continuity equations*

The Stokes equations (1) and (2) are solved using a Galerkin least-squares (GLS) method [12]. This method contains an additional pressure stabilization term compared with the standard Galerkin method. In such a way, the use of linear elements for both the velocity and pressure is permitted. The GLS variational formulation of the momentum-continuity equations is

$$\int_\Omega 2\eta\dot{\gamma}(\mathbf{u}) : \dot{\gamma}(\mathbf{v})\,\mathrm{d}\Omega - \int_\Omega p\nabla\cdot\mathbf{v}\,\mathrm{d}\Omega + \int_\Omega \nabla\cdot\mathbf{u}q\,\mathrm{d}\Omega$$
$$+\sum_K \int_{\Omega_K} \{\nabla p - \nabla\cdot[2\eta\dot{\gamma}(\mathbf{u})]\}\cdot\tau_u\nabla q\,\mathrm{d}\Omega_K = 0 \tag{6}$$

The stabilization parameter τ_u is defined as

$$\tau_u = \frac{m_k h_K^2}{4\eta} \tag{7}$$

where h_K is the size of the element K and m_k is a coefficient commonly considered $1/3$ for linear elements.

2.7. *Energy equation*

For polymers, the Prandtl number takes large values. Therefore, during the filling, the energy equation is dominated by the convection. However, cooling generated by the heat lost through walls, coupled with a low material diffusivity, generates high temperature gradients in direction normal to the wall. The solution algorithm must correctly represent both advective and diffusive mechanism. In this work a GLS/GGLS method is used to solve for the temperature. The GLS [12] term stabilizes the convection, whereas the GGLS contribution [14] deals with the presence of sharp boundary layers.

The GLS/GGLS formulation of Equation (3) is

$$\int_\Omega \rho c_p \left(\frac{T-T_0}{\Delta t} + \mathbf{u}\cdot\nabla T\right) w \,\mathrm{d}\Omega + \int_\Omega k\nabla T\cdot\nabla w \,\mathrm{d}\Omega - \int_\Omega 2\eta\dot{\gamma}^2 w \,\mathrm{d}\Omega$$
$$+\sum_K \int_{\Omega_K} \left[\rho c_p \left(\frac{T-T_0}{\Delta t} + \mathbf{u}\cdot\nabla T\right) - \nabla\cdot(k\nabla T) - 2\eta\dot{\gamma}^2\right] \tau_T \rho c_p \mathbf{u}\cdot\nabla w \,\mathrm{d}\Omega_K$$
$$+\sum_K \int_{\Omega_K} \nabla\left[\rho c_p \left(\frac{T-T_0}{\Delta t} + \mathbf{u}\cdot\nabla T\right) - \nabla\cdot(k\nabla T) - 2\eta\dot{\gamma}^2\right] \tau_\nabla \nabla w \,\mathrm{d}\Omega_K$$
$$= \int_{\Gamma_{\text{mould}}} h_c(T - T_{\text{mould}}) w \,\mathrm{d}\Gamma \tag{8}$$

Note that the stabilization terms are integrated only over the element interiors. The stabilization parameter τ_T is defined as in References [13, 24]

$$\tau_T = \left[\left(\frac{2\rho c_p}{\Delta t}\right)^2 + \left(\frac{2\rho c_p|\mathbf{u}|}{h_K}\right)^2 + \left(\frac{4k}{m_k h_K^2}\right)^2\right]^{-1/2} \tag{9}$$

The definition of the stabilization parameter τ_∇, as from Reference [14], is

$$\tau_\nabla = \frac{h_K^2}{6}\bar{\xi} \tag{10}$$

where

$$\bar{\xi} = \frac{cosh(\sqrt{6\alpha}) + 2}{cosh(\sqrt{6\alpha}) - 1} - \frac{1}{\alpha} \tag{11}$$

$$\alpha = \frac{(\rho c_p/\Delta t){h_K}^2}{6k} \tag{12}$$

with h_K the element size. The dimensionless parameter $\bar{\xi}$ tends towards unity for very large values of α and to $1/2$ for α much smaller than unity. The contribution of the transient term to the stabilization acts as an artificial conductivity, given by

$$k_a = \frac{\rho c_p}{\Delta t}\tau_\nabla = \frac{(\rho c_p/\Delta t){h_K}^2}{6}\bar{\xi} \tag{13}$$

2.8. Front tracking equations

The front tracking equations are discretized using an SUPG finite element method. SUPG provides smooth solutions when the convective part of the equation is dominant, as is in the present case. The variational formulation is given by

$$\int_\Omega \left(\frac{\partial F}{\partial t} + \mathbf{u}\cdot\nabla F\right) v \,\mathrm{d}\Omega + \sum_K \int_{\Omega_K} \left(\frac{\partial F}{\partial t} + \mathbf{u}\cdot\nabla F\right) \tau_F(\mathbf{u}\cdot\nabla v) \,\mathrm{d}\Omega_K = 0 \tag{14}$$

In the absence of diffusion the stabilization coefficient τ_F is defined as

$$\tau_F = \frac{h_K}{2|\mathbf{u}|} \tag{15}$$

The front tracking functions are discretized using linear elements. They are reinitialized after each time step to insure mass conservation of the skin and core polymers.

3. APPLICATIONS

3.1. Co-injection of a rectangular plate

The mould cavity is a centrally gated rectangular plate with dimensions of $76 \times 164 \times 7$mm as shown in Figure 1. The sprue geometry has parallel sides with a slight taper and a constant height. The experimental trials were carried out in a 150-ton Engel co-injection machine. The horizontal and vertical barrel/screw plasticizing units are used to feed the skin and core materials, respectively, to the co-injection head. The materials are injected sequentially in the mould through a single nozzle equipped with a check valve, which controls the amount of material entering the mould. A given percentage of the skin material is first injected in the cavity, followed by the injection of the core material. The material used for both skin and core is an injection grade polycarbonate Caliber 200-14 supplied by The Dow Chemical Company. For visualization purposes, a red pigment is added to the core material. The polymer viscosity is modelled with the Cross-WLF model

$$\eta(T, \dot{\gamma}, p) = \frac{\eta_0(T, p)}{1 + \left(\dfrac{\eta_0(T, p)|\dot{\gamma}|}{\tau^*}\right)^{1-n}} \tag{16}$$

$$\eta_0(T, p) = D_1 \exp\left[-\frac{A_1(T - T^*)}{A_2 + (T - T^*)}\right] \tag{17}$$

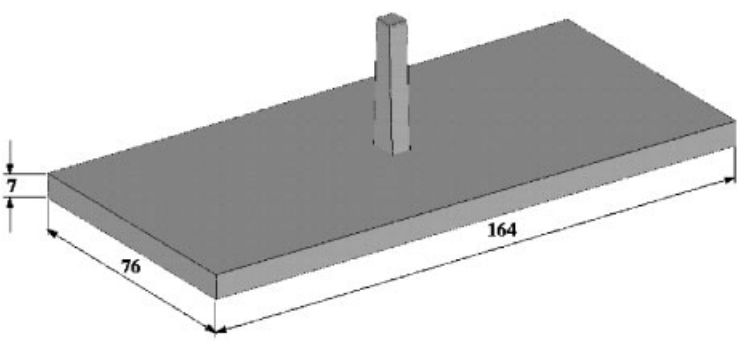

Figure 1. Geometry of the centre gated plate.

where

$$T^*(p) = D_2 + D_3 p \tag{18}$$

and

$$A_2(p) = \widetilde{A}_2 + D_3 p \tag{19}$$

The rate of deformation $|\dot{\gamma}|$ is computed from the strain rate tensor as $|\dot{\gamma}| = \sqrt{2\dot{\gamma} : \dot{\gamma}}$. Model constants used for the numerical simulation are summarized in Table II. Density, specific heat and thermal conductivity were considered constant, equal to 1162 kg/m^3, 2000 J/(kg °C), and 0.25 W/(m °C), respectively.

Numerical solutions were obtained on a cluster of Pentium III processors running at 1 GHz. The mesh consists of 44 850 nodes and 199 440 tetrahedral elements. Given the segregated nature of the solution algorithm, the maximum CFL number at the melt/air interface is limited to unity, and a typical solution needs about 150 time steps for the filling period. Convective terms are dominant in the energy and front tracking equations and the algorithm solves them using fractional time steps, thus increasing the accuracy but also the computational time. Solutions are obtained in about 5 hours when using 8 processors. Computations were carried out for different skin/core ratio, skin/core injection temperatures and skin/core injection speeds and the results were compared with the moulded parts. Process conditions and simulation results are summarized in Table III. The temperature of the injected melt was set at either 300 or 250 °C, while the mould temperature was set at 90 °C. Screw speed was considered either 20 or 50 mm/s. At the lower injection speed, filling of the plate takes 3.5 s, while at the faster speed it takes 1.4 s. The reference case has a skin/core ratio of 80/20 and the same injection temperature (300 °C) and injection speed (20 mm/s) for both skin and core.

A typical series of experimental short shots using single material injection is shown in Figure 2. Comparison is made with the numerical predictions for shots of 10–60 mm. The part is completely filled for a shot of about 72 mm. As can be seen the agreement between experiment and simulation is excellent. Figure 3 illustrates the solution of the co-injection process for the reference case. Front view and isometric view are shown. The skin polymer is plotted in transparency in order to allow for the core to be visible. The core material advances more rapidly in the direction corresponding to the plate length. Because the plate fills first in the width, the core penetrates less in this direction. The 3D solution of the co-injection process is able to predict the core shape in all directions. Most important, the residual skin thickness is computed and critical regions can be identified. In this case thin polymer skin is predicted in the region of the gate. The hot polymer is directed into the opposite wall and the skin thickness is very small at this location. Far from the centre, the core polymer penetrates by the mid-plane and the skin thickness is almost the same on top and bottom of the part.

Table II. Cross-WLF model constants for PC200.

Model constant	Value
n; τ^* (Pa)	0.18; 5.766×10^5
D_1 (Pa s); D_2(°C); D_3(°C/Pa)	3.46×10^6; 175.0; 0.0
A_1; $\widetilde{A}_2$(°C)	11.59; 33.98

Table III. Operating conditions and simulation results.

Condition	Skin/core ratio (vol.%)	Skin/core injection speed (mm/s)	Skin/core melt temperature (°C)	Delay time (s)	Core penetration length/width (mm)
Reference	80/20	20/20	300/300	0	47.2/30.0
A	A(1): 90/10 A(2): 70/30 A(3): 60/40	20/20	300/300	0	29.2/23.4 61.2/32.8 72.9/30.0
B	80/20	B(1): 20/50 B(2): 50/20 B(3): 50/50	300/300	0	46.7/29.8 45.0/29.6 44.3/29.4
C	80/20	20/20	C(1): 300/250 C(2): 250/300 C(3): 250/250	0	44.8/30.4 51.8/28.9 48.4/29.7
D	80/20	20/20	300/300	D(1): 1 D(2): 2 D(3): 4	50.5/30.1 52.3/30.3 56.0/30.6

Figures 4 (experiment) and 5 (numerical simulation) illustrate the change in the solution when the ratio skin/core polymer is varied. The skin/core ratio varies from 90/10 to 60/40. As more core material is injected in the cavity the core penetrates deeper inside the skin. Core penetration changes mostly in the length of the plate as the filling during core injection occurs mostly in this direction.

Experimental and numerical core penetration in length and width directions are compared in Figures 6–9. The effect of changing the skin/core ratio (Figure 6), the injection speed (Figure 7), the injection temperature (Figure 8), and the core injection delay (Figure 9) is investigated. As expected, Figure 6 indicates that a deeper core penetration is observed for a higher ratio core/skin materials. The effect of the injection speed is shown in Figure 7. By increasing the injection speed the temperature of the polymer increases because of the shear heating and also of the smaller cooling time. The net effect is that a faster filling (i.e. higher temperature) determines a higher core thickness and therefore a shorter core penetration length. A similar effect is observed when the skin/core temperature is varied (Figure 8). The mean injection temperature is computed by using 80% of the skin value and 20% of the core value. A lower temperature determines a thinner core (thicker skin) and hence a deeper core penetration. Note however that changes in skin and core temperature have opposite effects. A lower core temperature determines a higher viscosity core. Therefore, the core is thicker and the penetration length is shorter. Meanwhile, lower skin temperature determines a thicker skin and therefore deeper core penetration. Changing the core injection delay (Figure 9) has a similar effect on the solution. Increasing the delay is equivalent to a lower skin temperature and hence deeper core penetration.

This results indicate a good agreement between experiment and simulation except for cases C(2) and C(3) which present core instability in the experiment. Both numerical simulation and experiment indicate that core penetration increases at longer filling times (Figure 7), at

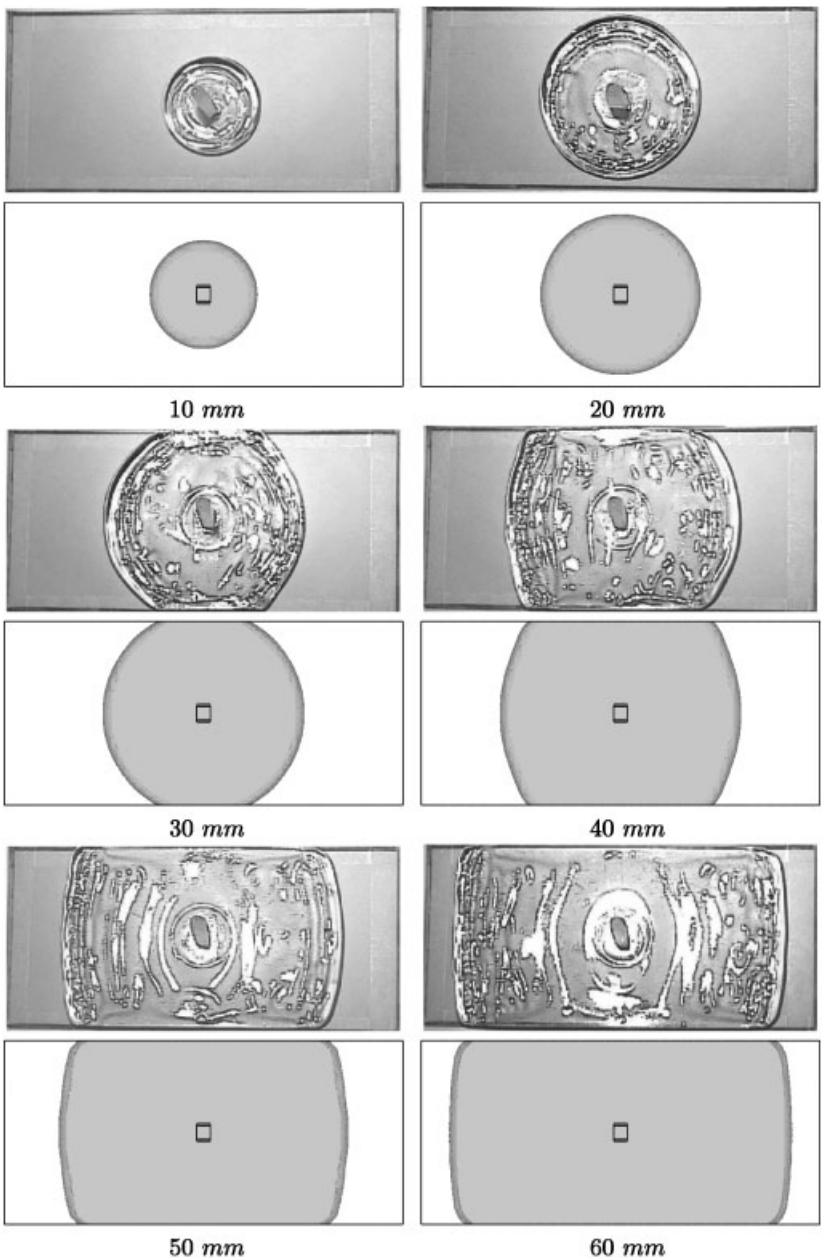

Figure 2. Comparison of experimental and numerical short shots.

higher core temperature (reference case compared with C(1) and C(2) compared with C(3)), at smaller skin temperature (reference case compared with C(2) and C(1) compared with C(3)), and at larger core injection delay (Figure 9).

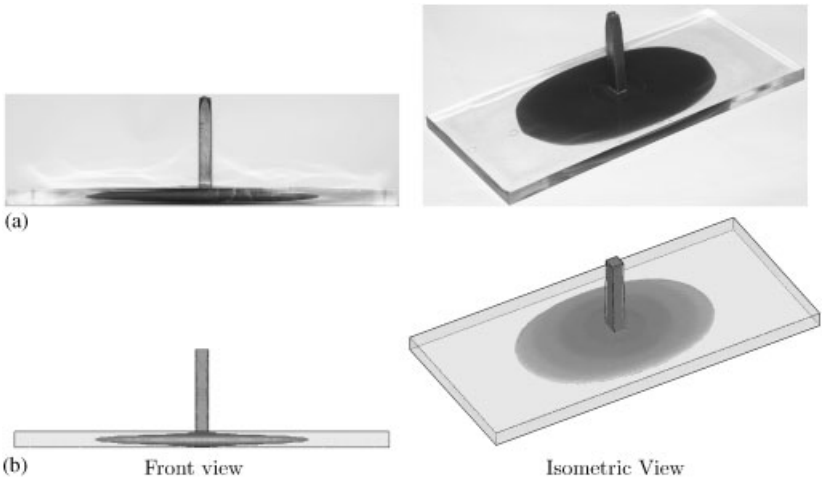

Figure 3. (a) Experimental; and (b) simulated results for the co-injected plate in the reference case.

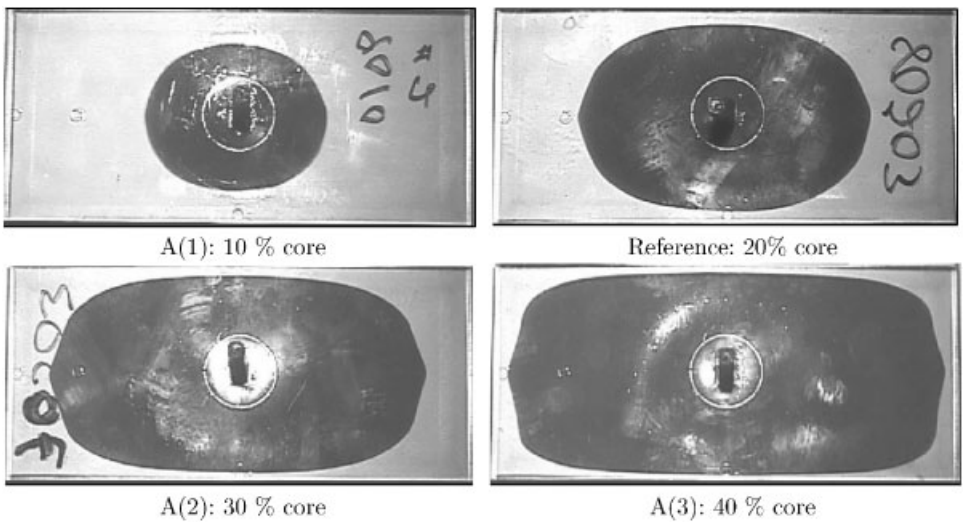

Figure 4. Co-injected parts for different ratios skin/core polymers for 20/20 mm/s injection speed and 300/300 °C injection temperature.

3.2. *Co-injection in a spiral-flow mould*

This application was the object of an experimental study by Watanabe *et al.* [25]. The mould has a spiral-flow cavity with 20 mm width and 2 mm thickness (see Figure 10). The moulding material for both skin and core is PC (Panlite L-1225L). Material properties for the numerical simulation were: density $\rho = 1200\,\mathrm{kg/m^3}$, specific heat $c_p = 2000\,\mathrm{J/(kg\,^\circ C)}$, and thermal conductivity $k = 0.25\,\mathrm{W/(m\,^\circ C)}$. The viscosity is modelled by the Cross-WLF model equations

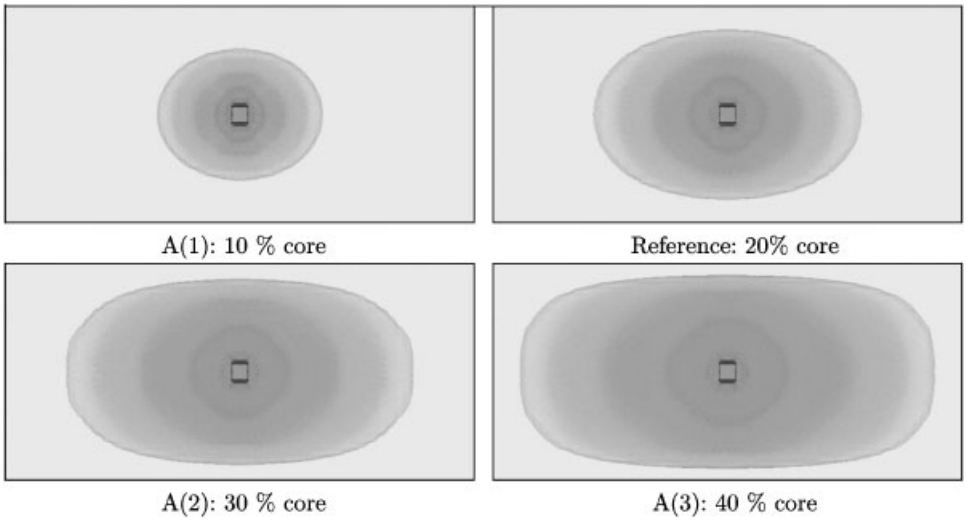

Figure 5. Numerical solutions of co-injected parts for different ratios skin/core polymers for 20/20 mm/s injection speed and 300/300 °C injection temperature.

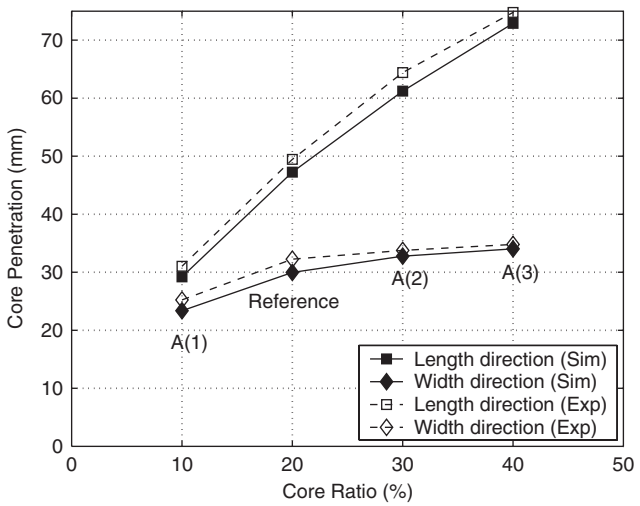

Figure 6. Core penetration at various skin/core ratios.

(16)–(19) with the constants as given in Table IV. The melt is injected at 300 °C and the mould is kept at 80 °C. The core and skin materials were injected sequentially. The core material is injected at 0.7 s when the flow length of skin material is about 70 mm. The numerical solution for the skin and core flow length is compared with the experimental data of Watanabe *et al.* [25] in Figure 11. The numerical model results in very accurate predictions and indicates correctly the core expansion phase between $t = 1.7$ and 2.3 s. During

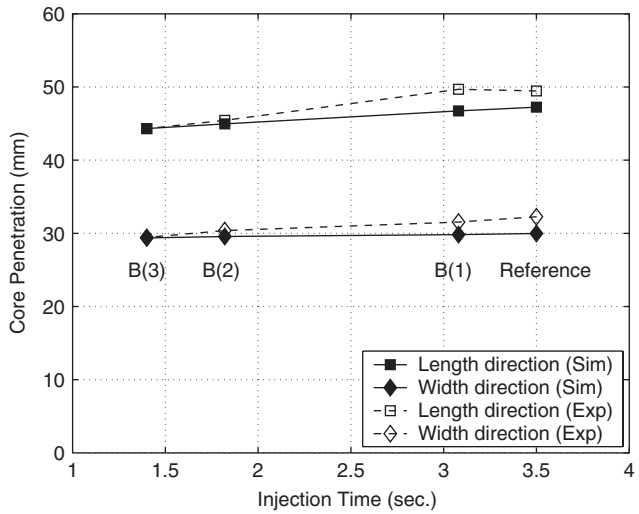

Figure 7. Core penetration at various injection speeds.

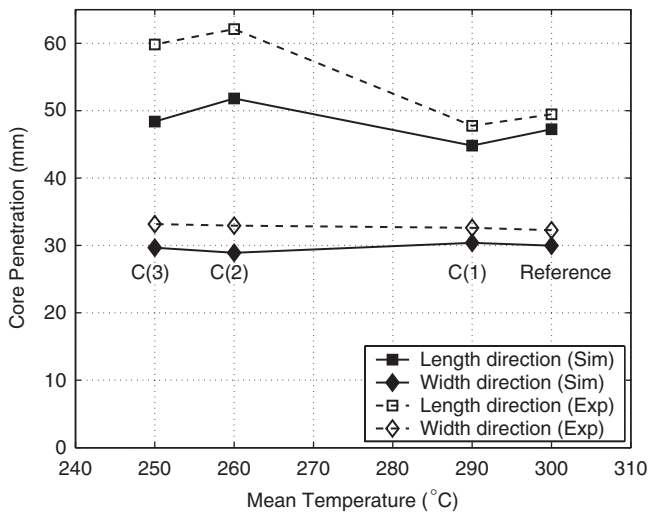

Figure 8. Core penetration at various injection temperatures.

this period the flow front of core and skin materials advance together without breakthrough. Breakthrough occurs at about $t = 2.3$ s as observed in the experiment. The numerical solution prior to breakthrough is shown in Figure 10 with the skin material plotted in transparency (lighter colour).

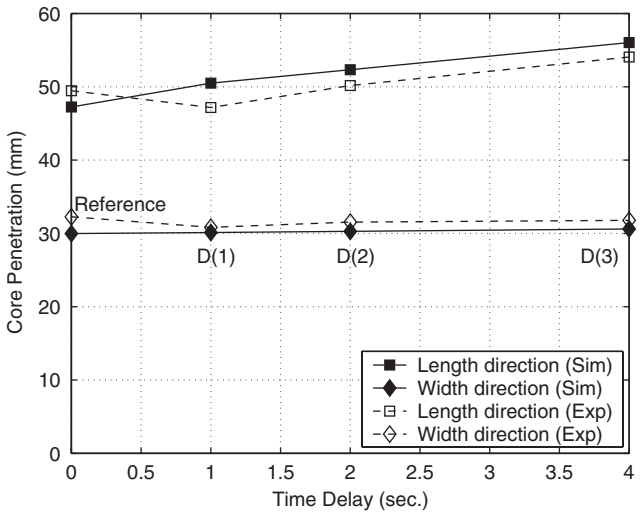

Figure 9. Core penetration at various core injection delays.

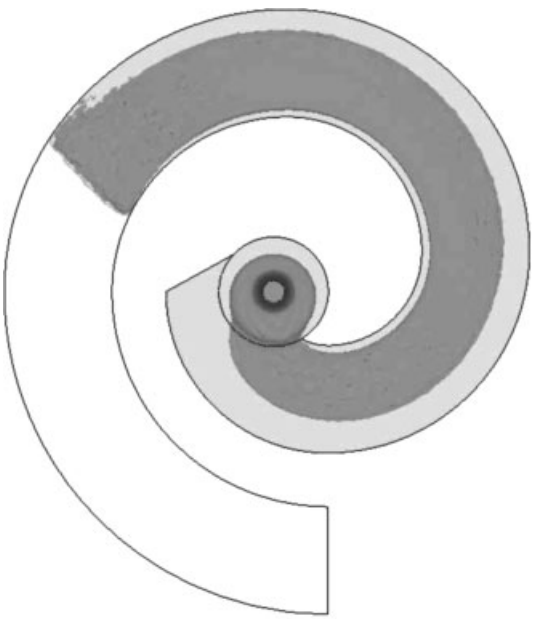

Figure 10. Spiral mould: core penetration prior to breakthrough occurrence ($t = 2.3$ s).

Table IV. Cross-WLF model constants for Panlite L-1225L.

Model constant	Value
n; τ^*(Pa)	0.12; 8.5×10^5
D_1(Pa s); D_2(°C); D_3(°C/Pa)	3.8×10^9; 175.0; 0.0
A_1; $\widetilde{A}_2$(°C)	22.0; 44.0

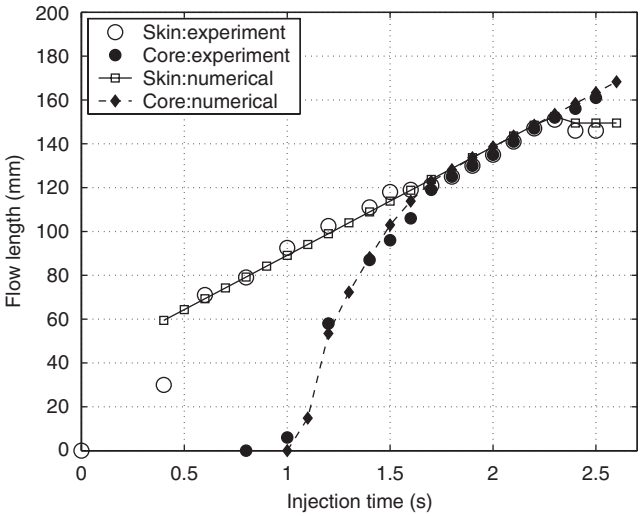

Figure 11. Skin and core position for spiral mould.

4. CONCLUSION

This work presents experimental and numerical results for the co-injection moulding process. The numerical approach provides the evolution of the polymer/air and skin/core polymer interfaces and the final shape and depth of the core polymer. Solutions were presented for a centre-gated plate for different skin/core injection speed and temperature and different ratios of the skin/core materials. The influence of the core injection delay was also investigated. Core penetration is influenced by the viscosities of skin and core, which in turn depend mostly on the temperature. Higher skin viscosity determines a thicker skin and hence deeper core penetration. Inversely, higher core viscosity determines a thicker core and a shorter core penetration.

The application to the case of the spiral-flow mould indicated the ability of the numerical approach to predict complex behaviour as the core expansion phase and the core material breaking through the skin material. The proposed numerical procedure works in the same manner for thin parts and for thick 3D parts, and provides all the needed information concerning the thickness of the skin polymer and the shape of the core material. Therefore it can be very useful in predicting the optimal moulding conditions for obtaining parts with specific characteristics.

REFERENCES

1. Garner PJ, Oxley DF. *British Patent No. 1,156, 217*, 1971.
2. Oxley DF, Sandiford DJH. Sandwich moulding. *Plastics and Polymers* 1971; **39**:288–292.
3. Eckardt H. How to develop a successful coinjection application. In *Proceedings of the 14th Annual Structural Foam Conference 1986*, SPI (ed.), Society of Plastics Industry, Boston, MA, 21–23 April 1986; 24–44.
4. Young SS, White JL, Clark ES, Oyanagi Y. A basic experimental study of sandwich injection moulding with sequential injection. *Polymer Engineering and Science* 1980; **20**(12):798–804.
5. Chen C, Hsu KF, Jung WR. Study of polymer melt flow during injection moulding using co-injection moulding technique. In *Proceedings of the ANTEC 1994*, Society of Plastics Engineers (ed.), Society of Plastics Engineers, San Francisco, CA, 1–5 May 1994; 671–679.
6. Turng LS, Wang VW, Wang KK. Numerical simulation of the coinjection moulding process. *Transactions of the ASME—Journal of Engineering Materials and Technology* 1993; **115**:48–53.
7. Chen SC, Hsu KF. Numerical simulation and experimental verification of melt front advancements in coinjection moulding process. *Numerical Heat Transfer*, *Part A* 1995; **28**:503–513.
8. Schlatter G, Davidoff A, Agassant JF, Vincent M. Numerical simulation of the sandwich injection moulding process. In *Proceedings of the ANTEC 1995*, Society of Plastics Engineers (ed.), Society of Plastics Engineers, Boston, MA, 7–11 May 1995; 456–459.
9. Lee DJ, Isayev AI, White JL. Simultaneous sandwich injection moulding: simulation and experiment. In *Proceedings of the ANTEC 1998*, Society of Plastics Engineers (ed.), Society of Plastics Engineers, Atlanta, GA, 26–30 April 1998; 346–350.
10. Schlatter G, Davidoff A, Agassant JF, Vincent M. An unsteady multifluid model: application to sandwich injection moulding process. *Polymer Engineering and Science* 1999; **39**(1):78–88.
11. Ilinca F, Hétu JF. Three-dimensional simulation of multi-material injection moulding: application to gas-assisted and co-injection moulding. *Polymer Engineering and Science* 2003; **43**(7):1415–1427.
12. Franca LP, Frey SL. Stabilized finite element methods: II. The incompressible Navier–Stokes equations. *Computer Methods in Applied Mechanics and Engineering* 1992; **99**:209–233.
13. Ilinca F, Hétu JF, Pelletier D. On stabilized finite element formulations for incompressible advective–diffusive transport and fluid flow problems. *Computer Methods in Applied Mechanics and Engineering* 2000; **188**: 235–255.
14. Franca LP, Dutra do Carmo EG. The Galerkin gradient least-squares method. *Computer Methods in Applied Mechanics and Engineering* 1989; **74**:41–54.
15. Ilinca F, Hétu JF. Galerkin gradient least-squares formulations for transient conduction heat transfer. *Computer Methods in Applied Mechanics and Engineering* 2002; **191**:3073–3097.
16. Ilinca F, Hétu JF. Three-dimensional filling and post-filling simulation of polymer injection moulding. *International Polymer Processing* 2001; **16**:291–301.
17. Ilinca F, Hétu JF, Derdouri A, Stevenson J. Metal injection moulding: 3D modelling of nonisothermal filling. *Polymer Engineering and Science* 2002; **42**(4):760–770.
18. Ilinca F, Hétu JF. Three-dimensional finite element solution of gas-assisted injection moulding. *International Journal for Numerical Methods in Engineering* 2002; **53**:2003–2017.
19. Baaijens FPT, Douven LFA. Calculation of flow-induced residual stresses in injection moulded products. *Applied Scientific Research* 1991; **48**:141–157.
20. Douven LFA. Towards the computation of properties of injection moulded products. *Ph.D. Thesis*, Technische Universiteit Eindhoven, 1991; 184.
21. Wimberger-Friedl R, Janeschitz-Kriegl H. Residual birefringence in injection moulded compact discs. *First International Conference on Electrical*, *Optical and Acoustic Properties of Polymers*, Canterbury, U.K., 1988; 22/1–22/10.
22. Janeschitz-Kriegl H. *Polymer Melt Rheology and Flow Birefrengence*. Springer: Berlin, 1983; 424–448.
23. Wu S. Surface and interfacial tensions of polymers, oligomers, plasticizers and organic pigments. *Polymer Handbook*, Brandup J, Immergut EH, Grulke EA (eds), 1991; 521–541.
24. Tezduyar TE, Aliabadi SK, Behr M, Mittal S. Massively parallel finite element simulation of compressible and incompressible flows. *Research Report 94-013*, Army High Performance Computing Research Center, Minneapolis, MN, 1994.
25. Watanabe D, Ishiaku US, Nagoaka T, Tomari K, Hamada H. Flow behaviour of sandwich injection moulding in sequential and simultaneous injection. *International Polymer Processing* 2003; **28**:199–203.

